ARMY RESEARCH LABORATORY

Embedded Carbon Nanotube Networks for Damage Precursor Detection

by Pranay Mishra, Asha Hall, and Michael Coatney

ARL-TR-6773 **January 2014**

NOTICES

Disclaimers

The findings in this report are not to be construed as an official Department of the Army position unless so designated by other authorized documents.

Citation of manufacturer's or trade names does not constitute an official endorsement or approval of the use thereof.

Destroy this report when it is no longer needed. Do not return it to the originator.

Army Research Laboratory
Aberdeen Proving Ground, MD 21005-5069

ARL-TR-6773 **January 2014**

Embedded Carbon Nanotube Networks for Damage Precursor Detection

Pranay Mishra
American Society for Engineering Education (ASEE),
College Qualified Leaders (CQL) Program

Asha Hall and Michael Coatney
Vehicle Technology Directorate, ARL

REPORT DOCUMENTATION PAGE	Form Approved OMB No. 0704-0188

1. REPORT DATE *(DD-MM-YYYY)*	2. REPORT TYPE	3. DATES COVERED (From - To)
January 2014	Final	1–31 July 2013

4. TITLE AND SUBTITLE
Embedded Carbon Nanotube Networks for Damage Precursor Detection

5a. CONTRACT NUMBER

5b. GRANT NUMBER

5c. PROGRAM ELEMENT NUMBER

6. AUTHOR(S)
Pranay Mishra,* Asha Hall, and Michael Coatney

5d. PROJECT NUMBER

5e. TASK NUMBER

5f. WORK UNIT NUMBER

7. PERFORMING ORGANIZATION NAME(S) AND ADDRESS(ES)
U.S. Army Research Laboratory
ATTN: RDRL-VTM
Aberdeen Proving Ground, MD 21005-5069

8. PERFORMING ORGANIZATION REPORT NUMBER
ARL-TR-6773

9. SPONSORING/MONITORING AGENCY NAME(S) AND ADDRESS(ES)

10. SPONSOR/MONITOR'S ACRONYM(S)

11. SPONSOR/MONITOR'S REPORT NUMBER(S)

12. DISTRIBUTION/AVAILABILITY STATEMENT
Approved for public release; distribution is unlimited.

13. SUPPLEMENTARY NOTES
*American Society for Engineering Education (ASEE), College Qualified Leaders Program, 1818 N. St. NW, Ste. 600, Washington, DC 20036

14. ABSTRACT
Current structural health monitoring efforts are limited by the finite number of localized points that can be analyzed. Because of their small size, carbon nanotubes can combine with materials without significantly affecting the original material properties. Adding carbon nanotubes into a material allows researchers to create a distributed conductive network within the material. As damage occurs within these materials, the electrical properties of this network change with it. In this study, Epon 863 (epoxy) dogbone specimens were fabricated with super-aligned multiwall carbon nanotubes for embedded sensing for damage precursor detection. The specimens were under cyclic fatigue loading as the electrical response was monitored. A four-point probe method was used to pass the current through the samples while recording the change in resistance. After the specimen underwent cyclic fatigue, a fractographic analysis was conducted to correlate the type of damage along with the change in resistance.

15. SUBJECT TERMS
structural health monitoring, carbon nanotube composite materials, cyclic fatigue, precursor damage, embedded sensing

16. SECURITY CLASSIFICATION OF:			17. LIMITATION OF ABSTRACT	18. NUMBER OF PAGES	19a. NAME OF RESPONSIBLE PERSON
a. REPORT	b. ABSTRACT	c. THIS PAGE			Asha Hall
Unclassified	Unclassified	Unclassified	UU	20	19b. TELEPHONE NUMBER (*Include area code*) 410-278-8036

Contents

List of Figures

List of Tables

1. Introduction/Background

Monetary issues play a significant role in how today's Army operates. A large portion of Army funding is directed toward operations and maintenance (O&M) costs, particularly when referencing vehicle O&M. Any damage that occurs to a vehicle means some part has to be repaired or replaced. Material state awareness is the process where a system will determine the vehicle health by providing indicators prior to failure. Such systems are meant to enhance reliability/safety while lowering maintenance costs by improving upon the operational efficiency of such structures.

In recent years the idea of in situ structural health monitoring (SHM) has been explored because of its multiple advantages, including better life cycle health management, enhanced performance, increased structural integrity, and reduced costs. The fusion of this data determines the vehicle health and its ability to perform a given mission. For example, civil engineering infrastructure has equipped bridges throughout the world with strain gages, accelerometers, and other sensors to collect data to detect how the materials fatigue with time. This well-established approach has correlated the degree of degradation to a time line for addressing the real-time critical health capabilities of the infrastructure.

Damage detection requires the comparison of two system states: identifying the existence and location of damage and using that data to determine the severity of damage.[1] In this report, our focus is to augment the SHM of the matrix material of composite with carbon nanotubes (CNTs) to detect the existence of degradation and also to identify the type of damage within the system. Our vision is to monitor a composite or matrix material damage on a microscale that otherwise could not be detected through other detection methods.

This project focuses on establishing a material state awareness system with CNT-reinforced epoxy. Epoxy is widely used in vehicles, particularly aerospace vehicles, where fiber-reinforced epoxy is integral to the structural materials. In 1999 Sandler et al.[2] demonstrated the conductive properties of CNT-reinforced epoxy in microscopic samples. Three years later Thostenson and Chou[3] created aligned nanocomposite films with 5 weight-percent (wt.%) of CNT that showed an increase in elastic modulus as well as tensile strength. In the following years groups such as Gojny et al.[4] have continued to show that double-walled carbon nanotube–reinforced epoxy has

[1]Worden, K., Farrar, C., Manson, R., Park, G. The Fundamental Axioms of Structural Health Monitoring. *Proceedings of the Royal Society* **2007**, *463* (2082), 1639–1664.

[2]Sandler, J.; Shaffer, M. S. P.; Prasse, T.; Bauhofer, W.; Schulte, K.; Windle, A. H. Development of a Dispersion Process for Carbon Nanotubes in an Epoxy Matrix and the Resulting Electrical Properties. *Polymer* **1999**, *40*, 5967–5971.

[3]Thostenson, E. T.; Chou, T.-W. Carbon Nanotube Networks: Sensing of Distributed Strain and Damage for Life Prediction and Self-Healing. *Advanced Materials* **2006**, *18*, 2837–2841.

[4]Gojny, F. H.; Wichmann, M. H. G.; Fiedler, B.; Bauhofer, W.; Schulte, K. Influence of Nano-Modification on the Mechanical and Electrical Properties of Conventional Fibre-Reinforced Composites. *Composites A* **2005**, *36*, 1525–1535.

increased tensile strength. Vadlamani et al.[5] used carbon black and CNT reinforcement to study resistance measurement techniques. This study will focus on resistance and strength changes within epoxy dogbone samples (with embedded super-aligned multiwall carbon nanotube to correlate load-induced damage with resistance measurements to create new SHM capabilities.

2. Experimental

In order to create tests samples an inverted dogbone cast was fabricated (figure 1) on an Objet Eden260V* three-dimensional printer using a Fullcure† 850 VeroGray polymer material. The inverted cast was then filled with Dow Corning 3120 room temperature vulcanizing rubber to create the final mold. The rubber was mixed with Tin NW Catalyst at a 10:1 ratio. The viscous liquid rubber mixture was poured into the inverted cast and cured for 7–12 h, after which time the rubber solidified (figure 2). The resin material consisted of two parts: Epon Resin 863 (part A) and an amidoamine curing agent (Epikure Curing Agent 3072, part B). The agents were mixed to a 100:38.5 ratio of Epon 863 to Epikure curing agent 3072. This was the resin used to create all of the samples. To prevent injury, specific steps were taken to carefully measure and mix the materials in a chemical hood. Once part A was measured out and poured into a beaker, the beaker was then placed on a hot plate 80 °C for 10–15 min while mixing with a magnetic stirring rod. Next, part B was slowly added to part A in the beaker for an additional 10 min while still on the hot plate reducing the temperature to 75 °C while continuously stirring to degas the mixture of any trapped air bubbles. It is important that all the air bubbles have been completely degassed from the mixture in order to ensure that porosity from air pockets do not weaken the structure. After all the bubbles were gone, the mixture is then poured into the rubber mold to create a pristine sample (figure 3). The resin cured within 24 h at room temperature.

[5]Gojny, F. H.; Wichmann, M. H. G.; Fiedler, B.; Bauhofer, W.; Schulte, K. Influence of Nano-Modification on the Mechanical and Electrical Properties of Conventional Fibre-Reinforced Composites. *Composites A* **2005**, *36*, 1525–1535.

*Eden260V is a registered trademark of Stratasys.

†Fullcure is a registered trademark of Stratasys.

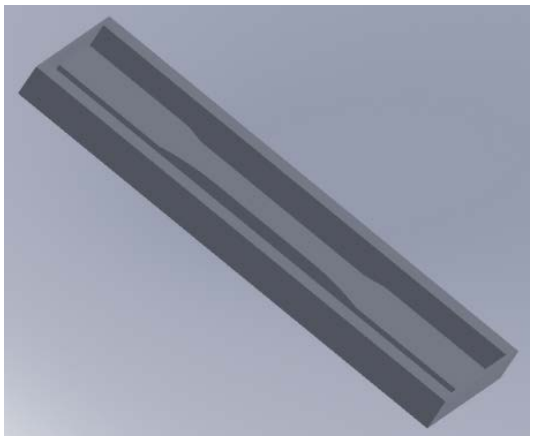

Figure 1. Solidworks rendering of inverted cast.

Figure 2. Rubber dogbone mold.

Figure 3. Fractured pristine sample.

For the embedded super-aligned multiwall carbon nanotube (MWCNT) sample, 50 strands of 15-cm-long MWCNT were placed on the top surface of a pristine resin dogbone sample and cured for 24 h (figure 4).

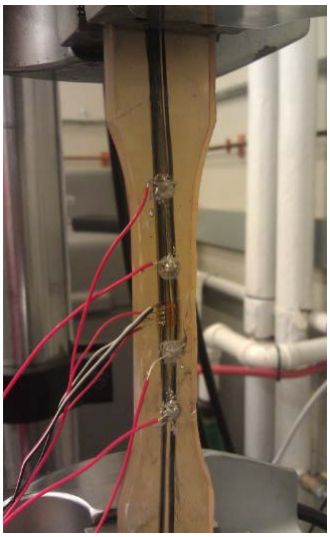

Figure 4. Super-aligned epoxy sample wired up in four-point probe configuration.

The objective of yield strength testing of pristine samples to embedded CNT samples is to see if the MWCNT reinforcement increased/decreased the tensile strength of the resin. A decrease in yield strength would make embedding MWCNT much less desirable, regardless of any other functionality it may provide. The stress-to-failure testing was done using an MTS load frame.

After establishing the yield strength, the resistance changes were correlated with the structural damage of the dogbone. A National Instruments data acquisition system with LabView was used to collect the load, strain, and resistance. Resistance measurements were done by employing a four-point method. Instead of constant current being passed through the outer dots, we used a function generator to pass a constant voltage of 400 mV through the 15-cm-long strands of the MWCNT network. Although there was a 26% drop in voltage from the outer dots to the inner dots, the drop remained constant under loading. Hence the constant voltage across the inner dots is different from the voltage passed through the outer dots. The leads were attached to the inner dots to measure current using a LabView program as the super-aligned MWCNT sample underwent fatigue testing. Prior to the fatigue testing, different voltages were passed through the inner dots and current readings were recorded to find the initial resistance of the sample. Strain measurements were recorded from strain gage data from a LabView program. The specimens were prepared by bonding tabs and a strain rosette to the specimen.

3. Results and Discussion

Cyclic fatigue experimentation was performed to assess the resistance deformation behavior of Epon 863 CNT embedded dogbone samples. Prior to the fatigue testing, three specimens were tested to obtain the average static strength of the specimens.

The stress-to-failure testing was done using an MTS load frame. Figure 5 contains the stress-strain curve of the pristine sample tensile test. The average Epon 863 dogbones had an elastic modulus of 5.806 GPa and an ultimate tensile strength of 65.64 MPa. The 0.2% offset yield strength was determined to be 32.078 MPa. From this stress-to-failure test, the cyclic fatigue load was determined to be 50% of the value of the failure load. Next, the specimens were tested in fatigue using load control and the direct loading approach. An R-ratio of 0.1 with a maximum load of 4 kips was chosen for the fatigue test. The procedure consisted of, first, ramping the load to 400 lb; second, cycling the load on the specimen at 5 Hz for the desired number of cycles or until failure occurred; and third, ramping the load down to 0 lb.

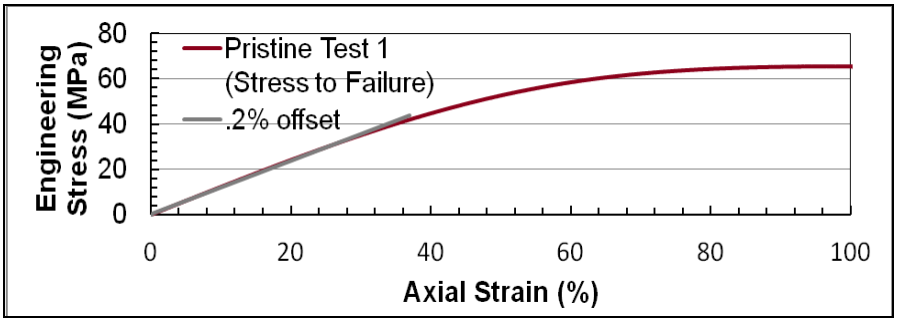

Figure 5. Stress-strain curve of the pristine sample during stress-to-failure test.

Monitoring the change in resistance measurements through a noninvasive electrical technique offers capability to identify the progression of damage. Initial resistance measurements were taken at different input voltages across the outer silver electrode dots. The specimen was loaded in tension, and the Poisson's ratio was recorded as 0.4269 for the MWCNT-embedded specimen prior to testing (figure 6). The corresponding inner silver electrode dot voltage drop was then recorded in table 1, as was the current across the inner silver electrode dots. For the 1000- and 10,000-cycle fatigue test, 400 mV was passed through the outer dots. As previously discussed, the voltage experienced a drop of 295 mV at the inner dots, and so for calculation purposes, this constant voltage was used in equation 1.

$$I = \frac{V}{R} \text{ (Ohm's law)} \tag{1}$$

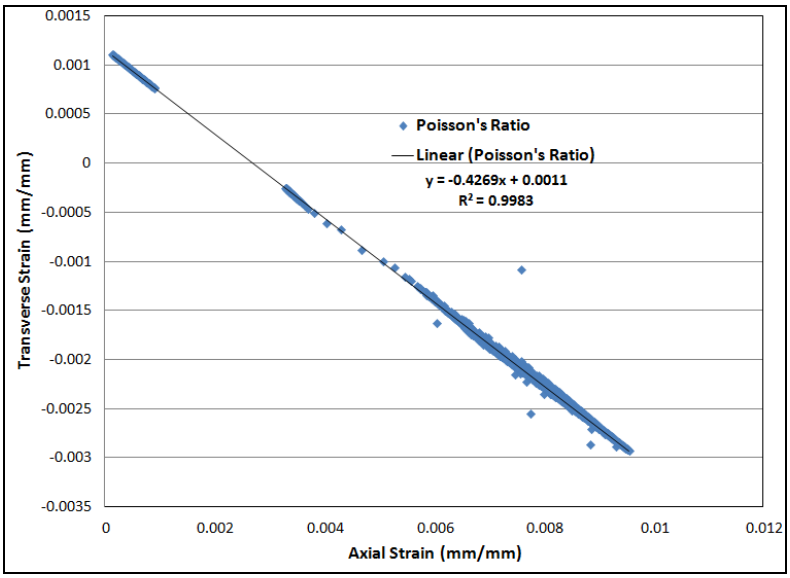

Figure 6. Transverse strain vs. axial strain indicating Poisson's ratio during 1000-cycle fatigue test.

Input Voltage mV (+)	Inner Dot Voltage mV (-)	Output Current mA (-)	Output Resistance ohms
100	73	0.15	486.6667
200	147	0.32	459.375
300	221	0.48	460.4167
400	295	0.64	460.9375
500	369	0.8	461.25
600	443	0.96	461.4583
700	517	1.13	457.5221
800	590	1.29	457.3643
900	664	1.45	457.931
1000	738	1.62	455.5556

Table 1. Voltage, current, and resistance values for the super-aligned sample prior to fatigue testing.

The super-aligned MWCNT sample was fatigue tested to 1000 cycles at a rate of 5 Hz. Figure 7 shows how the stress and current both changed versus percent axial strain as the sample went through the 1000 cycles that ranged from 19 to 28 MPa. The resistance plotted below the stress varies through a high and low range as each cycle is completed, ranging between 2735 and 2844 mA. Equation 1 is used to calculate resistance, as seen in figure 7. With the increase in stress or

strain, there are sharp spikes in resistance. The variation of resistance could be contributed to the cyclic nature of the testing, as it goes from an increase in load back down to zero load. As depicted in figure 8, over time, as the strain on the sample changes, the resistance value increases or decreases with a maximum change in 109 ohm.

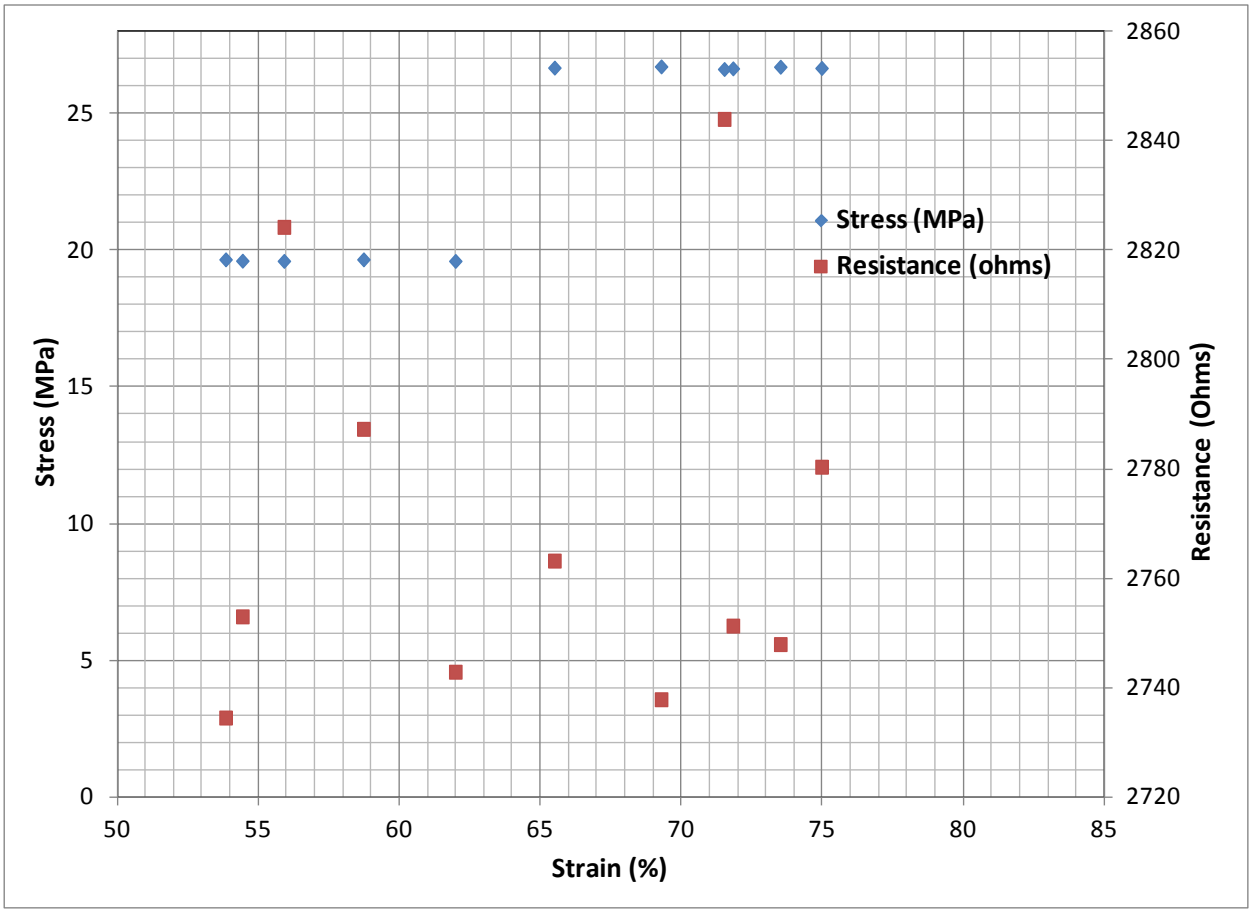

Figure 7. Stress and resistance values for the 1000-cycle fatigue test vs. strain percentage.

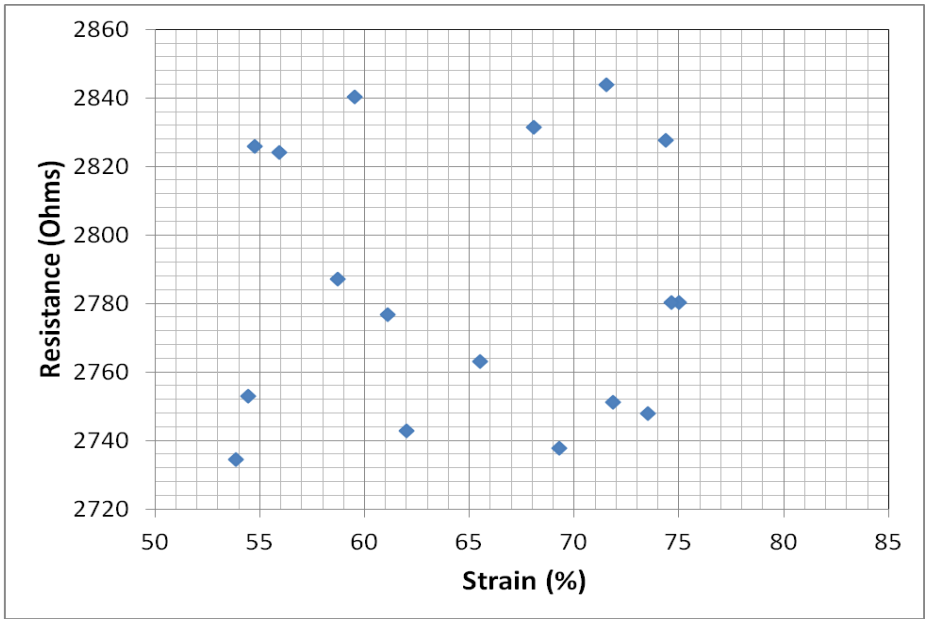

Figure 8. Resistance values for the 10,000-cycle fatigue test vs. strain percentage.

Figure 8 shows the change in resistance versus strain percentage. The observed stress in the 10,000-cycle test ranged from 17.5 to 28 MPa. The sample was fatigued for 10,000 cycles at a rate of 4 Hz. The fatigue test did not hit completion as the sample fractured near 3200 cycles. As shown in figure 9, there is an increase in resistance as the load is cycled; this increase indicates microcracking that may be oriented normal to the direction of the applied load. The difference is attributed to the lower cycling rate of the second fatigue test. At 4 Hz there is more time for each cycle to be completed, so the lower bound for the stress could drop more than during a rate of 4 Hz. The current in this test once again ranged between 0.104 and 0.110 mA. As done previously, equation 1 was used to calculate the resistance of the sample during the fatigue test as seen in figures 7 and 8. The resistance values also have a maximum amplitude value of 90 ohm.

A fractographic analysis was performed to evaluate the damage sites that corresponded to a change in resistance readings. A scanning electron microscope (SEM) image of the cracks formed in the sample is shown in figure 10. The fractographic analysis reveals significant cracking of the resin that would contribute to a sharp change in the resistance values. After fracture, the current increases in value from 0.12 to 0.33 mA, while the resistance drops from 2750 to 950 ohm during the 10,000-cycle test. This is an example of how damage to the sample causes a change in the resistance.

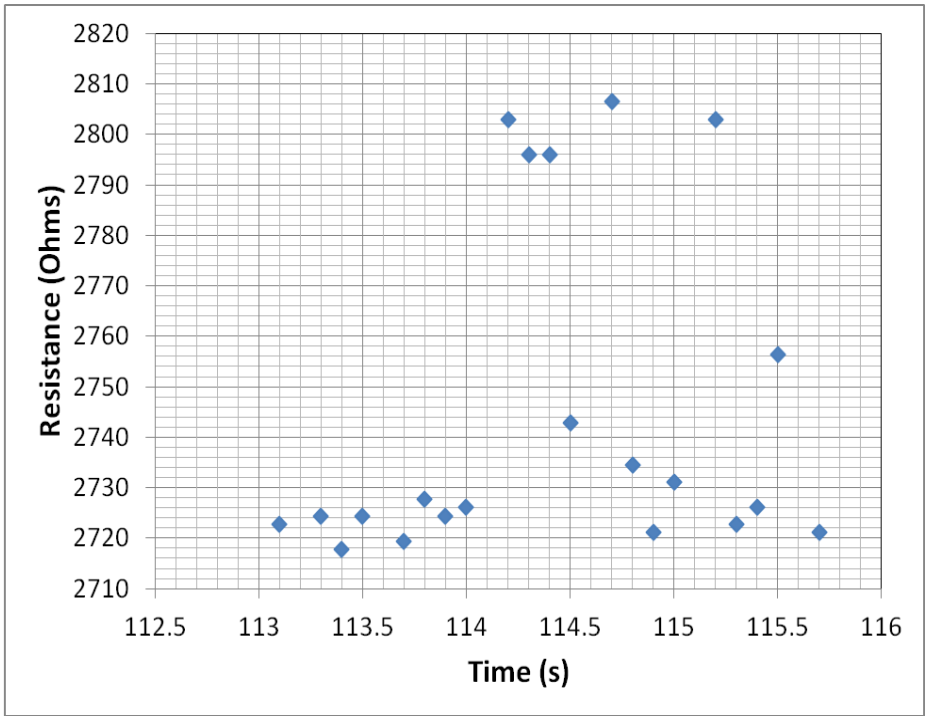

Figure 9. Resistance values for the 10,000-cycle fatigue test vs. time.

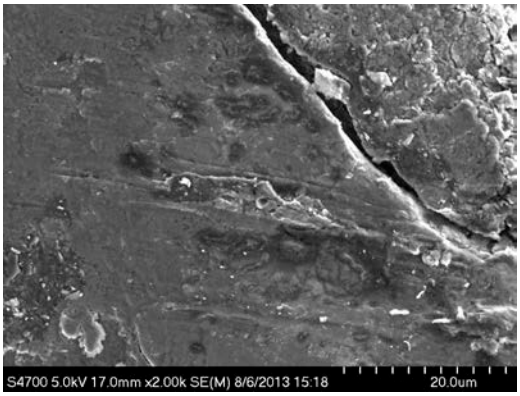

Figure 10. SEM image of cracks after fracture of super-aligned sample.

4. Summary and Conclusions

Fatigue testing has conclusively shown that the resistance of super-aligned MWCNT-reinforced epoxy will change when an induced load is placed upon it. During both the 1000- and the 10,000-cycle tests (before fracture), as the stress on the sample changed, the resistance would vary by as much as 109 and 90 ohm, respectively. After a severe damage event, such as a

fracture, the epoxy sample was still conductive and its resistance decreased by 65.5%. The results provide evidence that the conductive properties of MWCNT-reinforced epoxy will alter due to stress and damage; these factors make MWCNT reinforcement a viable option for damage progression. Future work will entail MWCNT sensing through the thickness of the specimen to accurately detect an onset and progression of the damage through the material.

Bibliography

Alexopoulos, N. D.; Bartholome, C.; Poulin, P.; Marioli-Riga, Z. Structural Health Monitoring of Glass Fiber Reinforced Composites Using Embedded Carbon Nanotube (CNT) Fibers. *Composites Science and Technology* **2009**, *70* (2), 260–271.

Baughman, R. H., Continuous Carbon Nanotube Composite Fibers: Properties, Potential Applications, and Problems. *Journal of Materials Chemistry* **2004**, *14*, 1–3

Bezryadin A.; Verschueren, A.; Tans, S.; Dekker, C. Multiprobe Transport Experiments on Individual Single-Wall Carbon Nanotubes. *Physical Review Letters* **1998**, *80*, 4036–4039.

Bily, M. A; Kwon, Y. W.; Pollak, R. D. Study of Composite Interface Fracture and Crack Growth Monitoring Using Carbon Nanotubes. *Applied Composite Materials* **2010**, *17* (4), *347–362.*

Kane, C. L.; Mele, E. J. Size, Shape, and Low Energy Electronic Structure of Carbon Nanotubes. *Physical Review Letters* **1997**, *78*, 1932–1935.

Li, H.; Qu, J. Smart Concrete, Sensors and Self-Sensing Concrete Structures. *Key Engineering Materials* **2009**, *400–402*, 69–80.

Li, H.; Xiao, H.-Q.; Qu, J.-P. Effect of Compressive Strain on Electrical-Resistivity of Carbon Black-Filled Cement Based Composites. *Cement and Concrete Composites* **2006**, *28*, 824–828.

Nardelli, M.; Bernholc, J. Mechanical Deformations and Coherent Transport in Carbon Nanotubes. *Physical Review B* **1998**, *60*, 16338–16341.

Nofar, M.; Hoa, S. V.; Pugh, M. D. Failure Detection and Monitoring in Polymer Matrix Composites Subjected to Static and Dynamic Loads Using Carbon Nanotube Networks. *Composites Science and Technology* **2009**, *69*, 1599–1606.

Park, J.-M.; Kim, D.-S.; Kim, S.-J.; Kim, P.-G.; Yoon, D.-J.; DeVries, K. L. Inherent Sensing and Interfacial Evaluation of Carbon Nanofiber and Nanotube/Epoxy Composites Using Electrical Resistance Measurement and Micromechanical Technique. *Composites: Part-B* **2007**, *38*, 847–861.

Paulson, S., Falvo, M.R., Snider, N., Helser, A., Hudson, T., Seeger, A., Taylor, R.M., Superfine, R., Washburn, S., In situ Resistance Measurements of Strained Carbon Nanotubes. *Applied Physics Letters* **1999**, *75* (19), 2936–2938.

Rejon L.; Rosas-Zavala, A.; Porcoyo-Calderon, J.; Castano, V. M. Percolation Phenomena in Carbon Black-Filled Polymeric Concrete. *Polymer Engineering and Science* **2000**, *40* (9), 2101–2104.

List of Symbols, Abbreviations, and Acronyms

A_0,	initial area (m^2)
E	elastic modulus (pascals)
F	force (newtons)
I	current (amperes)
L	final length (m)
L_0	initial length (m)
R	resistance (ohms)
ε	strain (mm/mm)
σ	stress (pascals)
V	voltage (volts)

NO. OF COPIES	ORGANIZATION
1 (PDF)	DEFENSE TECHNICAL INFORMATION CTR DTIC OCA
1 (PDF)	DIRECTOR US ARMY RESEARCH LAB IMAL HRA
1 (PDF)	DIRECTOR US ARMY RESEARCH LAB RDRL CIO LL
1 (PDF)	GOVT PRINTG OFC A MALHOTRA
5 (PDF)	RDRL VTM A HALL M COATNEY J RIDDICK M BUNDY D LE

INTENTIONALLY LEFT BLANK.